Hindawi
Advances in Civil Engineering
Volume 2021, Article ID 6637853, 15 pages
https://doi.org/10.1155/2021/6637853

Research Article

Bamboo/Wood Composites and Structures Shear and Normal Strain Distributions in Multilayer Composite Laminated Panels under Out-of-Plane Bending

Jan Niederwestberg,[1] **Jianhui Zhou**,[2] **Ying Hei Chui**,[1] **and Dongsheng Huang**[3]

[1]*Department of Civil & Environmental Engineering, University of Alberta, Edmonton T6G 1H9, Canada*
[2]*School of Engineering, University of Northern British Columbia, Prince George V2N 4Z9, Canada*
[3]*National Engineering Research Center of Biomaterials, Nanjing Forestry University, Nanjing 210037, China*

Correspondence should be addressed to Jan Niederwestberg; jan.niederwestberg@ualberta.ca

Received 11 November 2020; Revised 6 January 2021; Accepted 9 January 2021; Published 31 January 2021

Academic Editor: Hui Yao

Innovative mass timber panels, known as composite laminated panels (CLP), have been developed using lumber and laminated strand lumber (LSL) laminates. In this study, strain distributions of various 5-layer CLP and cross-laminated timber (CLT) were investigated by experimental and two modelling methods. Seven (7) different panel types were tested in third-point bending and short-span shear tests. During the tests, the digital imaging correlation (DIC) technique was used to measure the normal and shear strain in areas of interest. Evaluated component properties were used to determine strain distributions based on the shear analogy method and finite element (FE) modelling. The calculated theoretical strain distributions were compared with the DIC test results to evaluate the validity of strain distributions predicted by the analytical model (shear analogy) and numerical model (FE analysis). In addition, the influence of the test setup on the shear strain distribution was investigated. Results showed that the DIC strain distributions agreed well with the ones calculated by the shear analogy method and FE analysis. Both theoretical methods agree well with the test results in terms of strain distribution shape and magnitude. While the shear analogy method shows limitations when it comes to local strain close to the supports or gaps, the FE analysis reflects these strain shifts well. The findings support that the shear analogy is generally applicable for the stress and strain determination of CLP and CLT for structural design, while an FE analysis can be beneficial when it comes to the evaluation of localized stresses and strains. Due to the influence of compression at a support, the shear strain distribution near the support location is not symmetric. This is confirmed by the FE method.

1. Introduction

Cross laminated timber (CLT) and other mass timber panels like glue-, nail-, or dowel-laminated timber have become increasingly popular in the last decades. The increase in popularity can be a tribute to their large dimensions and cross sections, which allow for high levels of prefabrication and fast construction. Glue-, nail-, and dowel-laminated timber panels are manufactured from parallel lumber pieces connected to each other by either glue or nails of wooden dowels. Due to the parallel members, these panel types behave like beam elements in out-of-plane loading situations and can be considered as one-way elements. On the other hand, CLT panels are made from the commonly orthogonally arrangement of layers consisting of graded sawn lumber pieces that are glued to each other. The orthogonal arrangement of the layers lets CLT panels behave more like plates under out-of-plane loading, where loads can be transferred in both panel directions. Based on this, CLT panels can be considered two-way elements. However, the orthogonal arrangement of the layers leads to layers with radial-tangential cross section, which provide low shear modulus and strength. Due to this, CLT under out-of-plane loading is prone to high shear deformations and the so-called rolling shear failures when exposed to shear stresses perpendicular to the grain. Besides the low shear properties

of these cross-layers, gaps between the lumber pieces within these layers further promote shear deformation and rolling shear failures. Edge-gluing between adjacent laminates within a layer is beneficial but is not mandatory in the production of CLT [1].

Hybrid CLT with 3 layers made from European spruce and a European beech centre layer was tested in out-of-plane loading by [2]. Four-point bending tests and planar shear tests were used to determine the rolling shear properties of the beech core layer. Deflection measurements and strain gauges were used to determine the shear modulus of the beech. It was found that beech cross-layers improve the global shear behaviour of CLT significantly; both, shear modulus and strength improved; and the failure was shifted towards a longitudinal shear failure within the outer layers. In addition, the improved shear performance potentially allows for a simplified approach in design, treating the section as a rigid composite.

The bending and shear behaviour of 3-layer CLP and CLT formed from spruce-pine-fir (SPF) and laminated strand lumber (LSL) materials were investigated by [3]. Four (4) different lay-ups were evaluated in the program through bending and shear tests. The results showed that specimens with a LSL core layer and SPF outer layers had a 23% higher bending strength while reaching similar bending stiffness and a significant increase in shear stiffness compared to regular CLT. In addition, the bending failure was shifted from a rolling shear failure towards a flexural tensile failure. The short-span shear tests showed that the shear strength of specimens with a LSL core layer and SPF outer layers increased by 46% compared to regular CLT.

The use of oriented strand board (OSB) and spruce-pine-fir lumber in 3- and 5-layer CLP and CLT panels was evaluated by [4]. Ten different lay-ups were tested in the major and minor strength direction. The shear resistance and stress of the lay-ups were determined by experiments, shear analogy method, and finite element (FE) analysis. The results showed that the OSB provided higher mechanical properties compared to the lumber in the minor strength direction of the panels. Various failure modes were observed during bending tests. All hybrid CLT panels showed higher shear resistance compared to regular CLT. Furthermore, it was observed that the difference in shear resistance between the major and minor strength directions of hybrid CLT panels decreased with an increasing number of layers.

Three-layer CLP was investigated in [5]. The outer layers were made from Acacia lumber, while the core layer was formed from bamboo boards. Bending and shear tests were performed based on [6]. The tested CLP panels showed 176% higher bending stiffness and 37% higher bending strength compared to regular spruce-pine-fir CLT. The shear strength of the tested CLP was found to be 20% lower than the shear strength of spruce-pine-fir CLT. It was stated that the shear performance can potentially be improved if bamboo boards with higher strength are used.

Different analytical models were used by [7] to investigate the influence of shear deformation and the so-called rolling shear phenomenon in CLT in out-of-plane loading. The research compared results from the shear analogy method, the so-called Gamma method, and FE analysis with theoretical results assuming infinitely rigid transverse layers. The results showed that the influence of shear deformation can usually be neglected for most construction relevant cases (span-to-thickness ratio >30). For shorter panels, the influence of shear deformation should be considered. All of the utilized methods were capable of addressing the shear deformation and showed good agreement if appropriate input properties are used.

The influence of regular gaps between laminates within CLT layers was investigated by [8]. Laboratory test results were compared with results from FE analysis. The results from FE analysis showed good agreement with the laboratory tests. The work shows that the influence of small gaps can generally be neglected when determining the bending stiffness and that the influence of larger gaps can be addressed using a volume fraction approach. It was found that the influence of gaps between laminates on the in- and out-of-plane shear and torsional stiffness does not follow a volume fraction approach and that even narrow gaps lead to a significant reduction in stiffness.

The bending and shear properties of seven (7) different 5-layer CLP and CLT panel lay-ups were investigated in [9]. The bending properties were evaluated in third-point bending tests as well as modal tests while the shear properties were determined in short-span three-point bending tests. Compared to regular CLT, the CLP tests showed an increase of up to 43% of the bending stiffness, 87% of the bending strength, and up to 143% of the shear strength. The results were compared with the results calculated based on the shear analogy method. Similar to the findings in [3], the observed failure modes suggest that the use of structural composite lumber materials could avoid potential rolling shear failures. The digital imaging correlation (DIC) technique was employed to measure the strain developments in the thickness direction during bending and shear tests. The DIC results were briefly presented in [10].

All the research presented above addresses different structural CLP or CLT elements, but only some of it measures the strain behaviour of these elements during loading. While the work by [2, 4] evaluated local strain behaviour using strain gauges, only [10] utilized the DIC technique to evaluate strain distributions over the full height of the sections. Strain gauges are commonly used to evaluate the strain in the cross-layers of CLT and CLP elements. Due to the local nature of strain gauges, strain gauges located on these cross-layers cannot usually detect the influence of support conditions on the strain distribution, which is addressed in this research. The research [4, 7, 8] shows that FE analysis is well suited for determining strain, stress, and deflection of CLT and CLP panels. Nevertheless, the works do not address the effects of rapid local changes in loading.

Both the shear analogy method and FE modelling are currently adopted for the structural design of CLT building. The shear analogy method is a user-friendly analytical method, which is applicable for both CLT and CLP panels with the advantages in computational efficiency. FE modelling is well known to handle complicated geometry and load cases. The tests conducted in [9, 10] provided the

experimental data for the work presented herein, which aims to compare the shear and normal strains between DIC measurements and predictions by shear analogy method and FE modelling. The results will provide insights into the structural design of CLT members under out-of-plane loads.

2. Materials and Methods

As mentioned above, some of the materials, specimen preparation, test procedures, and test results were previously presented in [10]. Therefore, the used materials, the specimen preparation, and test procedures are only described here briefly as more detailed information can be found in [10]. In addition to the brief descriptions related to the laboratory tests and the analysis based on the shear analogy method, this section contains detailed information about the determination of the stress distributions and the modelling details in FE analysis.

2.1. Component Properties and Specimen Fabrication. Spruce-pine-fir (SPF) lumber of No. 2 grade and laminated strand lumber (LSL) were used to form the seven (7) symmetrically lay-up CLP and CLT panels. Before the CLP and CLT panels were formed, the moduli of elasticity (MOE) of the materials parallel to the grain were evaluated based on [6]. For the MOE values perpendicular to the grain and the shear moduli of the lumber, assumptions were made. The MOE perpendicular to the grain and the shear modulus parallel to the grain were estimated based on ratios of 1/16 and 1/30 of the MOE parallel to the grain of the lumber as suggested by [11]. The shear modulus perpendicular to the grain was assumed based on test results published in [12]. The MOE perpendicular to the grain of the LSL was assumed based on a ratio of 1/8 of the MOE parallel to the grain of the LSL [13]. The planar shear properties of the LSL were evaluated based on [14]. Table 1 presents the material properties of the lumber and LSL.

Seven (7) different CLP and CLT lay-ups were formed from the lumber and LSL. The panels were manufactured using a one-component polyurethane adhesive applied to one face only at a spread rate of 220 g/m^2. Due to the low moisture content of the LSL, the LSL surfaces were misted with water (32 g/m^2) before the gluing process to facilitate the curing of the adhesive. A bonding pressure of 1.38 N/mm^2 was applied to the assemblies. The panels were stored after gluing for at least 24 h before cutting the panels into test specimens. Two lay-ups were formed with but joints within LSL layers. Like the edges of the lumber pieces within a layer, these butt joints were formed without the application of adhesive. Figure 1 shows a butt joint within LSL layers. From the panels, which were about 2750 mm long, 1219 mm wide, and 184 mm thick, shear and bending specimens were cut. Shear specimens were cut to dimensions of 200 mm width and 1200 mm length. Test specimens for lay-ups with butt joints were cut in a way that the butt joints were located at the centre of the specimen. The bending specimens were cut to a width of 200 mm. Table 2 presents the different lay-ups,

Table 1: Component properties of lumber and LSL materials.

Material	Index	MC (%)	Density (kg/m^3)	MOE (N/mm^2)		Shear modulus (N/mm^2)	
				//	⊥	//	⊥
Lumber	Count	18	36	36	—	—	—
	Mean	7.4	470	10494	350*	656*	120*
	SE	0.05	5.0	243	—	—	—
LSL	Count	22	44	44	—	6	6
	Mean	3.4	644	9520	1190*	463	200
	SE	0.03	3.0	130	—	26.7	7.6

*Values based on assumptions.

Figure 1: Butt joints in the 2nd and 4th layer of a 5-layer A1a specimen.

Table 2: Five-layer CLP and CLT lay-ups ("T" = timber, "L" = LSL).

ID	Lay-up	Layer orientation	Shear tests	Bending tests
A1	T-L-L-L-T	//-//-//-//-//	8	13
A1a	T-L*-L-L*-T	//-//*-//-//*-//	8	16
A1b	T-L-L*-L-T	//-//-//*-//-//	8	14
B1	L-T-L-T-L	//-⊥-//-⊥-//	6	12
B2	L-T-L-T-L	//-//-//-//-//	6	14
C1	T-T-T-T-T	//-⊥-//-⊥-//	2	4
C2	T-T-T-T-T	⊥-//-⊥-//-⊥	2	4

*Layer contained a centred butt joint in LSL layer.

indicates the layer orientations, and provides the number of test specimens tested.

Before the shear and bending tests were performed, high contrast speckle patterns were applied onto the specimens. These speckle patterns allowed the digital imaging correlation (DIC) software to track the displacement of recognizable shapes and patterns based on photos taken during the loading process. By comparing the location of the recognizable patterns and shapes within the consecutively taken pictures with a reference picture taken before loading, the DIC software is capable of measuring displacement and strain of the laminate materials. Further information about DIC technique can be found in [15]. The shear test specimens were prepared with one speckle area, located over a support to measure the shear strain with minimum interference from bending strain. Two speckle areas were applied to the bending test specimens: one to evaluate maximum normal strain in the shear-free zone at the centre of the span and the other on one side halfway between a support and the

nearest loading point to evaluate the shear strain unaffected by the supports. Figure 2 shows a picture of the shear test setup and the speckle pattern as well as a shear force diagram. The shear speckle area is indicated by a red rectangle. Figure 3 shows a picture of the third-point bending tests and the applied speckle areas as well as a shear force and bending moment diagram. The shear speckle area is indicated by a red square while the bending speckle area is indicated by a green square.

2.2. Test Procedures. The shear and bending tests were performed based on [6] in test setups recommended in [16]. The shear tests were performed as short-span centre-point load shear tests at a span of 1000 mm (span-to-depth ratio = 5.5) and at a displacement rate of 2 mm/min. A total of 40 shear tests were performed. For the bending tests, a third-point bending test setup was employed at a test span of 2500 mm (span-to-depth ratio = 13.6), and tests were performed at a displacement rate of 4 mm/min. A total of 77 bending tests were undertaken. During the shear and bending tests, the applied load was recorded. In addition, two DIC cameras were focused on each speckle area and pictures were taken every two seconds and the recorded load was automatically correlated to the taken pictures.

2.3. Digital Imaging Correlation Analysis. The commercial DIC software VIC-3D [17] was used to analyse the DIC data. In the analysis, the relative displacements of the speckles within the DIC pictures are used to determine the strain across the speckled area. The software allows the user to define a specific path for which the strain values can be extracted, which are then plotted with respect to the location along the defined path. Here, the strain data extracted from the DIC data is directly used, only minor recalibrations were undertaken to centre the strain data over the cross section height. In addition, it should be noted that since VIC-3D uses the Lagrange strain tensors to calculate the shear strain, which is half of the engineering shear strain, the shear strain values were converted into engineering shear strain values. Shear and bending stress distributions can be determined based on the measured strain distributions using equations (1) and (2), respectively:

$$\tau_{(z)} = G_{(z)}\gamma_{(z)}, \tag{1}$$

where $\tau_{(z)}$ is the shear stress at location z in N/mm^2, $G_{(z)}$ is shear modulus at location z in N/mm^2, $\gamma_{(z)}$ is the shear strain at location z, and z is the distance of the location of interest to the neutral axis in mm:

$$\sigma_{(z)} = E_{(z)}\varepsilon_{(z)}, \tag{2}$$

where $\sigma_{(z)}$ is the bending stress at location z in N/mm^2, $E_{(z)}$ is the MOE at location z in N/mm^2, and $\varepsilon_{(z)}$ is the normal strain at location z.

To ensure that the strain data was taken from within the elastic range of the lay-ups, the strain data was determined at a load of approximately 40% of the average failure load of the corresponding test group. The approximate 40% loading of the average failure loads are presented in Table 3, where F_u is the failure load. For the bending tests, F_u represents the total load, not the individual loads.

While the DIC technique provides useful information on the shear and normal strain distributions, a direct conversion to stress distributions was not attempted in this research. In order to determine stress distributions, not only are the material properties required, but the layer boundaries need to be established precisely. Due to the measurement process with the speckle pattern on a white painted surface, the layer boundaries are hard to determine in some cases. While the boundaries could be estimated based on the known layer thicknesses, the location component of the strain distributions of the DIC measurements has to be considered less precise. The DIC strain is determined based on local averaging processes, which leads to uncertainty and missing values close to the specimen boundaries. This makes it difficult to precisely reference the strain to the layer boundaries. For specimens with lumber cross-layers, the large differences in the moduli of elasticity of the adjacent layers can lead to significant and unrealistic stress spikes in the associated stress distribution.

2.4. Shear Analogy Analysis. The shear analogy method is based on [18] and has been adopted in the CLT product standard [16] as well as in the Canadian timber design code CSA O86 [11] to determine the effective bending stiffness and shear stiffness of CLT. In order to determine the stress and strain distributions, the effective bending stiffness EI_{eff} of the cross section needs to be known. Here, the effective bending stiffness was determined for a shear-rigid equivalent system as described in [19]. The effective bending stiffness EI_{eff} of a rectangular cross section is determined based on fd3

$$EI_{\text{eff}} = \sum_{i}^{n} E_i \frac{b_i h_i^3}{12} + \sum_{i}^{n} E_i A_i z_{c,i}^2, \tag{3}$$

where EI_{eff} is the effective bending stiffness in Nmm^2, E_i is the MOE of layer i in N/mm^2, b_i and h_i are the width and thickness, respectively, of layer i in mm, A_i is the cross section area of layer i in mm^2, and $z_{c,i}$ is the distance of the centre of layer i to the neutral axis in mm.

While the strain distributions in the DIC tests can be directly extracted from the DIC software and then could be used to determine the stress distributions, the approach based on the shear analogy goes the opposite way. Here, the stress distributions are determined first and the strain distributions are then determined by transforming equations (1) and (2) towards $\gamma_{(z)}$ and $\varepsilon_{(z)}$, respectively. The shear stress distribution for an inhomogeneous cross section can be determined based on equation (4). Equation (5) presents an equation for the determination of the bending stress distribution of an inhomogeneous cross section:

$$\tau_{(z)} = \frac{V \sum E_{(z)} S_{(z)}}{EI_{\text{eff}} b_{(z)}}, \tag{4}$$

where V is the shear force in N, $\sum E_{(z)} S_{(z)}$ is the MOE weighted static moment at location z in Nmm, and $b_{(z)}$ is the width of the element at location z in mm:

Figure 2: DIC area in shear test and related shear diagram.

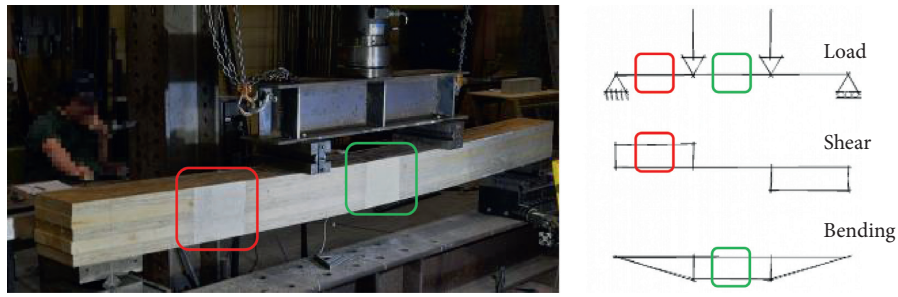

Figure 3: DIC areas in bending test and related shear and bending diagrams.

Table 3: Failure loads and loads for strain evaluation of lay-ups.

ID	Lay-up	Layer orientation	Shear tests		Bending tests	
			F_u (kN)	$0.4F_u$ (kN)	F_u (kN)	$0.4F_u$ (kN)
A1	T-L-L-L-T	//-//-//-//-//	138.7	55.5	86.0	34.4
A1a	T-L*-L-L*-T	//-//*-//-//*-//	136.5	54.6	75.6	30.2
A1b	T-L-L*-L-T	//-//-//*-//-//	148.9	59.5	79.8	31.9
B1	L-T-L-T-L	//-⊥-//-⊥-//	77.7	31.1	55.9	22.3
B2	L-T-L-T-L	//-//-//-//-//	178.1	71.2	108.1	43.2
C1	T-T-T-T-T	//-⊥-//-⊥-//	73.4	29.4	57.7	23.1
C2	T-T-T-T-T	⊥-//-⊥-//-⊥	37.4	15.0	28.5	11.4

F_u is the total failure load measured by a load cell attached to the cross-head.

$$\sigma_{(z)} = \frac{M}{EI_{\text{eff}}} E_{(z)} z, \tag{5}$$

where M is the bending moment in Nmm.

It should be noted that effective bending stiffness (EI_{eff}) was used for the determination of the strain values, while the relatively small span-to-thickness ratio of the bending tests suggests that the use of the apparent bending stiffness (EI_{app}), which includes the effects of shear deformation, might be more appropriate. Here, the effective bending stiffness (EI_{eff}) was used since it is a common published design parameter for mass timber panels and the general shape of the strain distributions would not be altered significantly, although there would be a slight difference in numerical values if EI_{app} was used instead.

The shear and bending stresses were determined based on a load of approximately 40% of the average failure load of the corresponding test group (see Table 3).

2.5. Finite Element Analysis. The FE analysis allows the direct extraction of strain and stress distributions. For the FE analysis, the commercial software Abaqus was employed [20]. The software allows creating three-dimensional models which can present the desired structure. Here, the CLP and CLT specimens were modelled by 3D deformable elements. It was assumed that the influence of gaps between adjacent pieces of lumber within layers running parallel to the test span can be neglected; each parallel layer was modelled by a single element. Layers that included gaps between pieces running perpendicular to the test span (A1a, A1b, B1, C1, and C2) were modelled with physical gaps (1 mm). The material properties used in the FE model were generally based on the properties evaluated in the component tests. Assumptions were made for the missing property characteristics. The properties were assigned direction based on the property orientations within the lay-ups. It should be noted that the lumber cross-layer elements were assigned the property "Lumber ⊥." Here, the properties of the lumber were converted to the global directions of the FE model in order to be able to present FE colour contour plots, which are based on global local systems. Therefore, the property directions of the lumber cross-layers needed to be changed

to match the other materials. Table 4 presents the material properties used in the FE models.

The bond between layers was assumed to be rigid; therefore, the layers were tied together in the FE models. In order to allow the extraction of the strain and stress data at similar locations as used in the laboratory tests, partitions were created in the model at the locations of interest. The general mesh size was chosen to be about half the layer thickness. Only in the areas of interest, the mesh size was redefined to 1/9 of the layer thickness to increase the data resolution. It should be noted that the redefined mesh was chosen for the purpose of resolution and that no convergence tests were conducted for the peak strain values. The boundary conditions were applied to reflect the boundary conditions of the laboratory tests. In order to simulate the influence of the support and loading plates, steel plates were added to the model, to which the boundary conditions and loads were applied. Similar to the laboratory shear tests, the supports in the FE shear model were not free to rotate, while the supports in the bending tests FE model were not restrained and were allowed to rotate freely. The contacts between all elements were defined as hard contacts in the normal direction of the surfaces other than the tied surfaces between layers and a friction coefficient of 0.3 was assigned of the tangential behaviour. The applied load level used in the analysis was 40% of the average failure load of the corresponding test group (see Table 3). Figure 4 shows the FE models for the CLT shear and bending test specimen C1. The locations of the shear related results are shown by red lines and the location of the bending strain results is indicated by a yellow line.

3. Results and Discussion

In the following, the results from the digital imaging correlation (DIC) strain measurements, the shear analogy (SA), and the FE analysis are presented. All results were obtained at a load of about 40% of the failure loads of the respective specimens in the related test setups as indicated in Table 3. The following graphs show colour contour plots from the DIC and FE evaluations, as well as strain diagrams presenting data evaluated based on DIC, shear analogy (SA) method, and finite element (FE) analysis. The locations of the strain evaluations in the DIC and FE contour plots tests are indicated by black dashed lines. The associated strain distributions were evaluated based on a chosen reference line within the software. It should be noted that the legends associated with the DIC colour contour plots are based in the full contour plot areas. The FE strain distributions were measured at the outer surface of the models. The colours within the DIC and FE contour plots might not match, and the plots are presented in order to show the strain distributions over the sections.

3.1. Shear Strain in Shear Tests. As shown in Figures 2 and 4, the shear strain measurements from the shear tests were evaluated close to the support areas. Figure 5 presents the data for the lay-ups A1, A1a, and A1b. Here, contour plots are shown from A1 only since all three lay-ups are almost identical, which reflects in the contour plots as well as the diagrams. Figures 6–9 show the information for lay-ups B1, B2, C1, and C2, respectively.

In general, it can be said that the DIC and FE colour contour plots match each other fairly well for all specimens. It should be noted that the shear strain in the DIC contour plot is presented as Lagrange strain tensors and therefore the strain values in the DIC contour plot legends are about half of the FE strain at the corresponding locations. High strain zones are located in similar areas of the contour plots. It can be seen that gaps between laminates (B1, C1, and C2) show high strain areas within the DIC contour plots, while the gaps show less significantly in the FE contour plots. The reason for this is likely the DIC evaluation method. As mentioned earlier, DIC determines the strain based on averaged relative movements. In the DIC analysis, the two boundaries and the related speckles are optically connected as they are used as reference points for each other. When gaps widen during loading, the speckles on the two boundaries of the gaps lead to high measured strain in the DIC. In the FE analysis, the boundaries of the gaps are not used as reference points for the determination of the strain values and thereby the strain values show less pronounce in the contour plots. In all diagrams, it can be observed that both DIC and FE data show asymmetrical strain distributions with respect to the centre of the cross sections ($z = 0$ mm) with higher strain towards the bottom lumber-to-LVL glueline followed by a step in strain. The asymmetric shape of the shear strain distributions from the shear tests was due to nearby reaction force. A locally induced load has a similar effect, leading to an asymmetrical shaped strain distribution with higher shear strain values on the side (z = positive or negative) of the induced load. Here, this was amplified since the boundary conditions were not free to rotate. The specimen rotates on the inner edges of the support, leading to a rapid decrease in internal forces within the cross section. While the FE distributions generally show similar characteristics as the DIC distributions, the SA distributions show a symmetrical shape, while still showing similar characteristics such as stepwise and parabolic characteristics. For A1, A1a, and A1b (Figure 5), it can be seen that the three specimens show similar strain distributions. It can be seen that the measured strain based on DIC exceeds both SA and FE calculated strains, but similar characteristics between DIC and FE strain distributions can be observed. For specimens B1, B2, C1, and C2 (Figures 6–9), the main characteristic of the shear strain distributions can be described as stepwise. Specimens with lumber cross-layers (B1, C1, and C2), especially, show strong steps, while the distribution specimen B2 shows both strong stepwise and parabolic characteristics.

3.2. Shear Strain in Bending Tests. As shown in Figures 3 and 4, the shear strain measurements from the bending tests were evaluated halfway between a support and the closest loading point. Figure 10 presents the data for the lay-ups A1, A1a, and A1b. Here, contour plots are shown from A1 only

Table 4: Material properties in finite element models.

Material	MOE (N/mm^2)			Shear modulus (N/mm^2)			Poisson ratio (—)		
	E_{11}	E_{22}	E_{33}	G_{12}	G_{13}	G_{23}	ν_{12}	ν_{13}	ν_{23}
Lumber	10494	350*	350*	656*	656*	120*	0.32*	0.35*	0.43*
Lumber ⊥	350*	10494	350*	656*	120*	656*	0.11*	0.43*	0.12*
LSL	9520	1904*	1904*	463	463	200	0.21*	0.13*	0.38*

*Values based on assumptions.

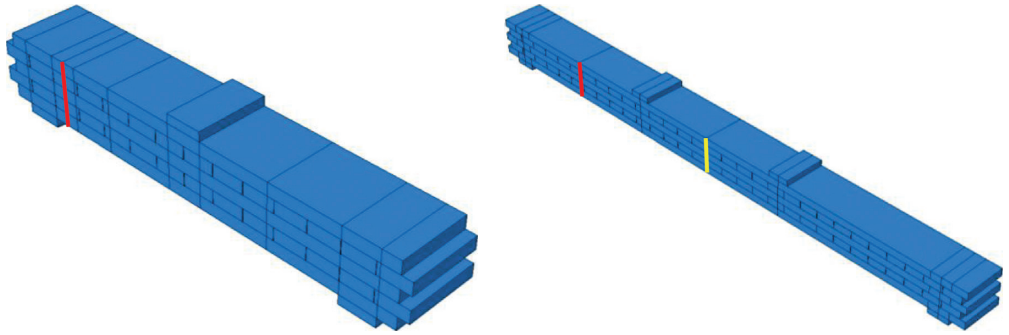

(a) (b)

Figure 4: Finite element models for shear and bending of CLT C1 (shear strain location = red lines, bending strain location = yellow line).

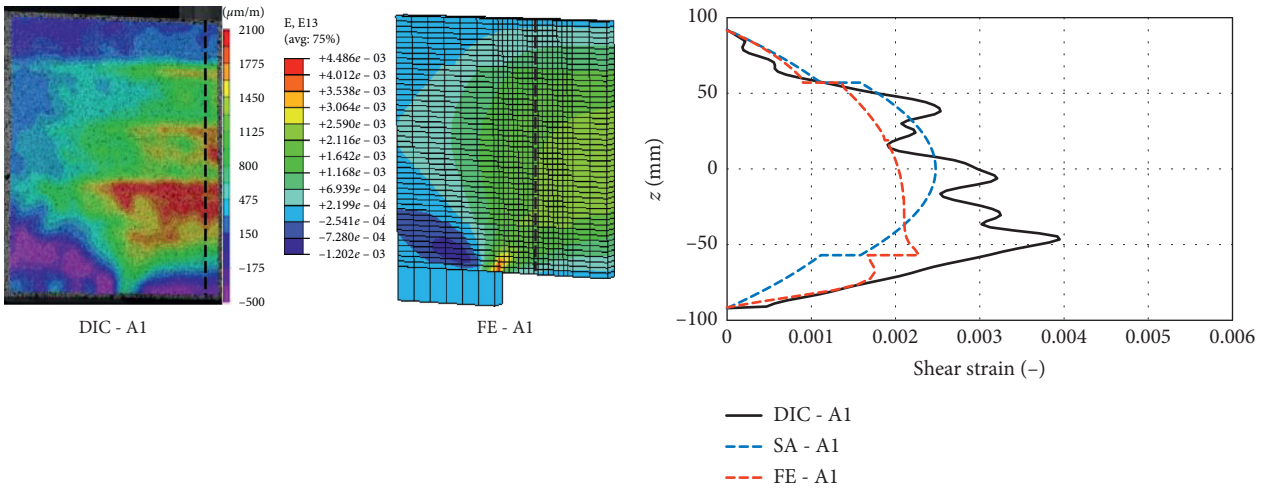

(a) (b)

Figure 5: Continued.

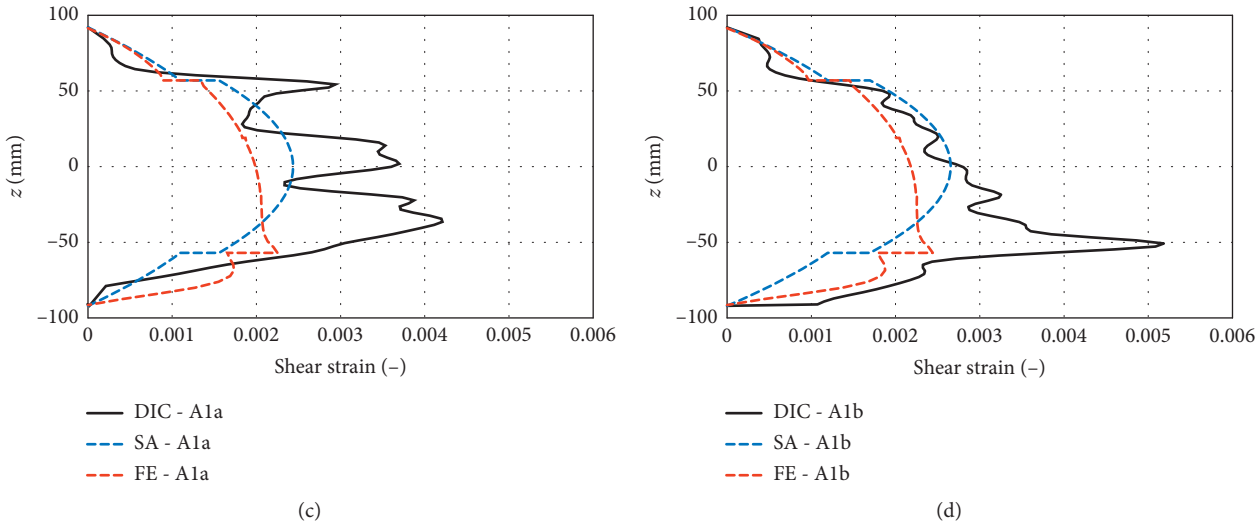

(c) (d)

Figure 5: Colour contour plots of A1 and shear strain distribution from shear tests for A1, A1a, and A1b.

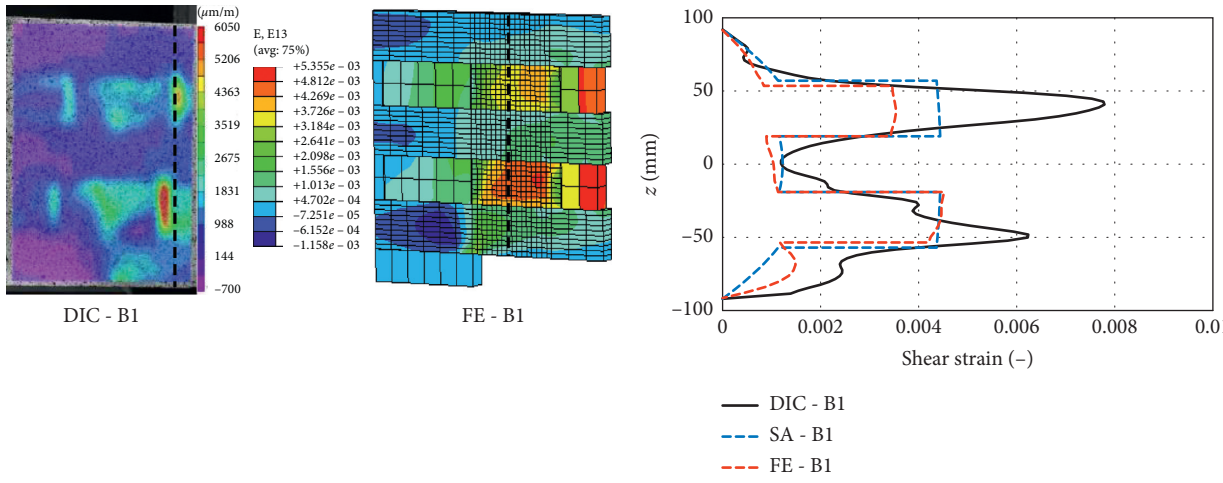

(a) (b)

Figure 6: Colour contour plots and shear strain distribution from shear tests for B1.

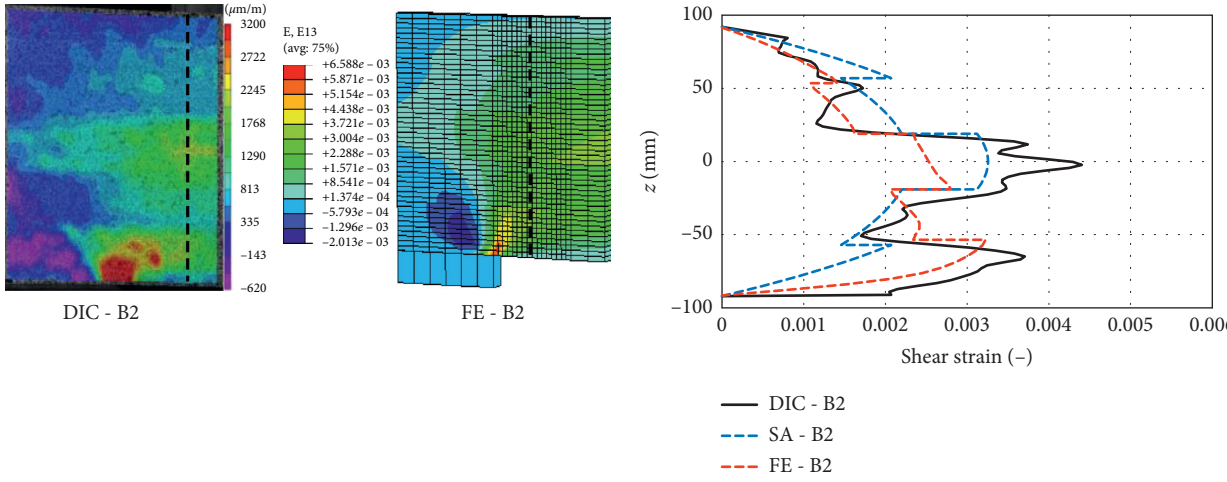

(a) (b)

Figure 7: Colour contour plots and shear strain distribution from shear tests for B2.

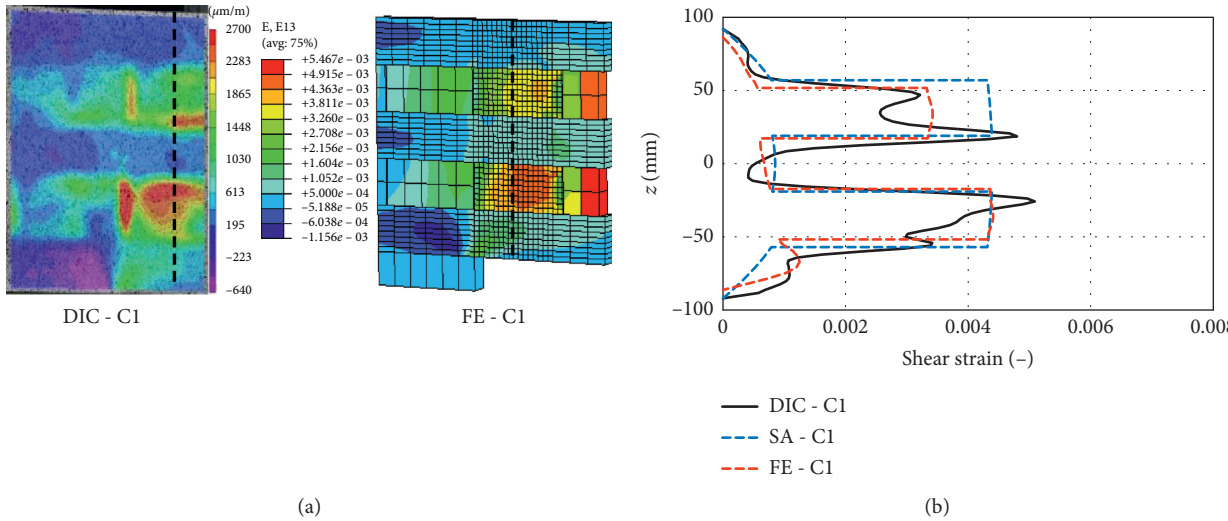

Figure 8: Colour contour plots and shear strain distribution from shear tests for C1.

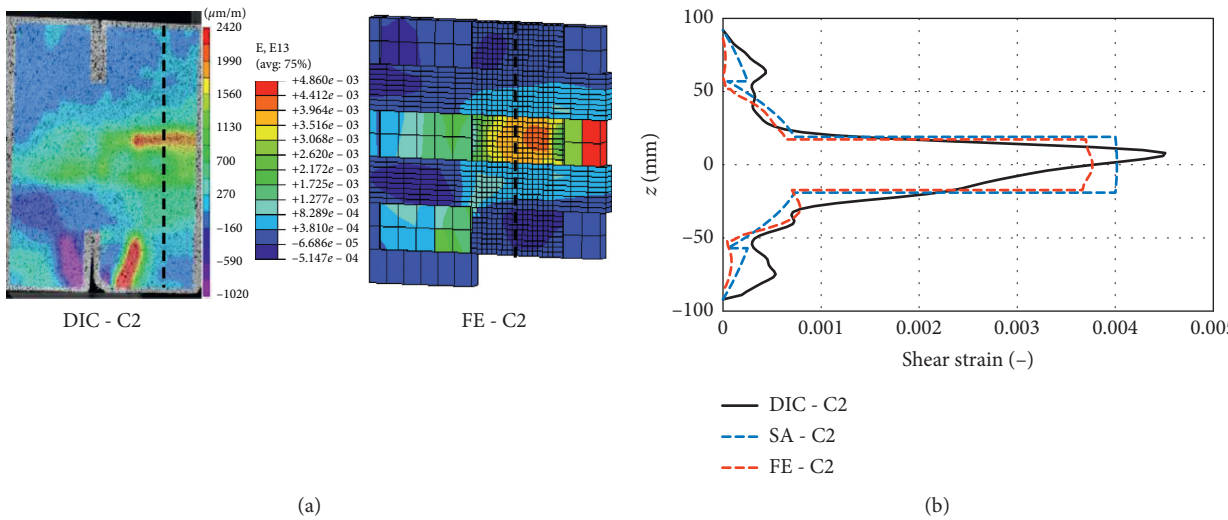

Figure 9: Colour contour plots and shear strain distribution from shear tests for C2.

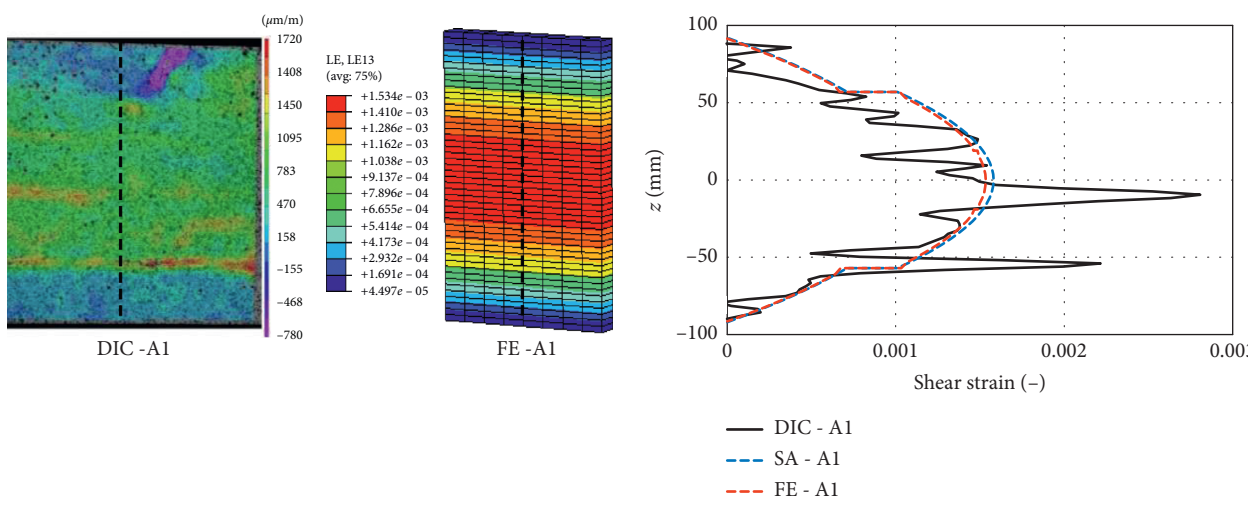

Figure 10: Continued.

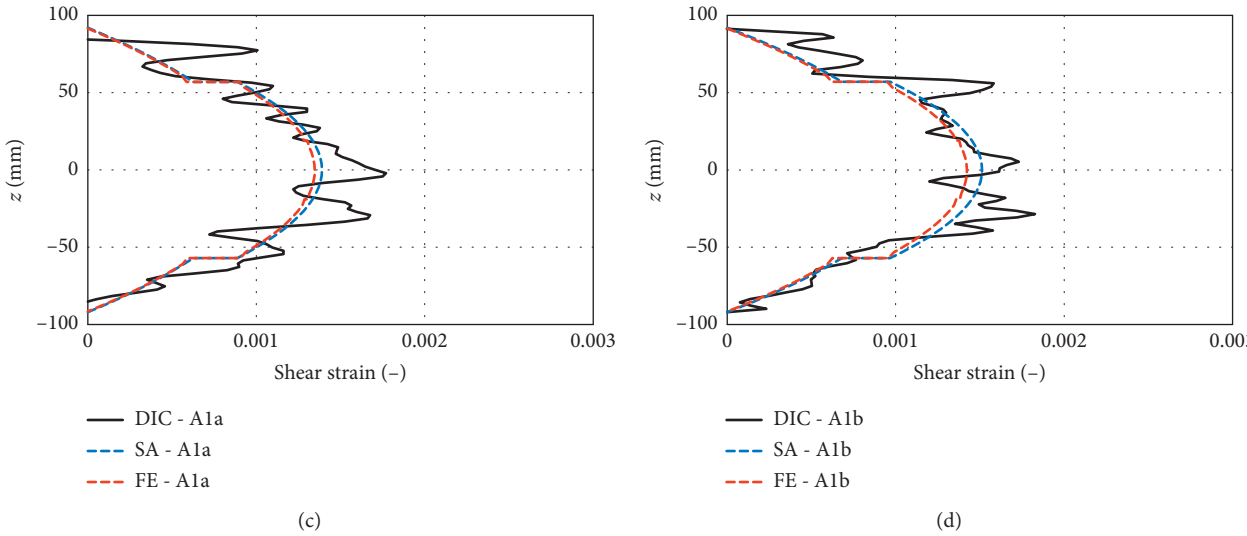

Figure 10: Colour contour plots of A1 and shear strain distribution from bending tests for A1, A1a, and A1b.

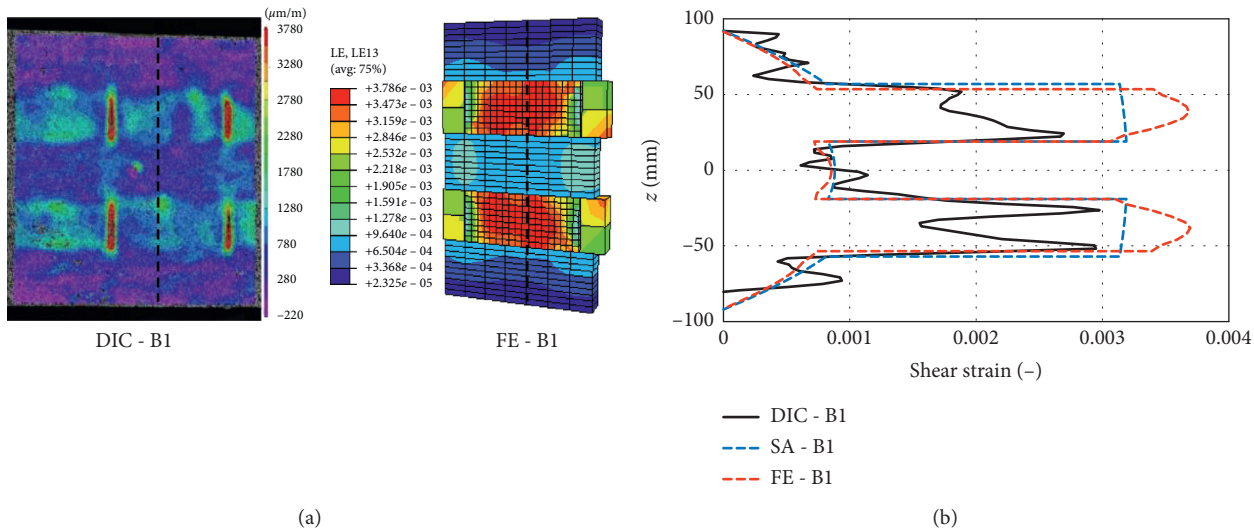

Figure 11: Colour contour plots and shear strain distribution from bending tests for B1.

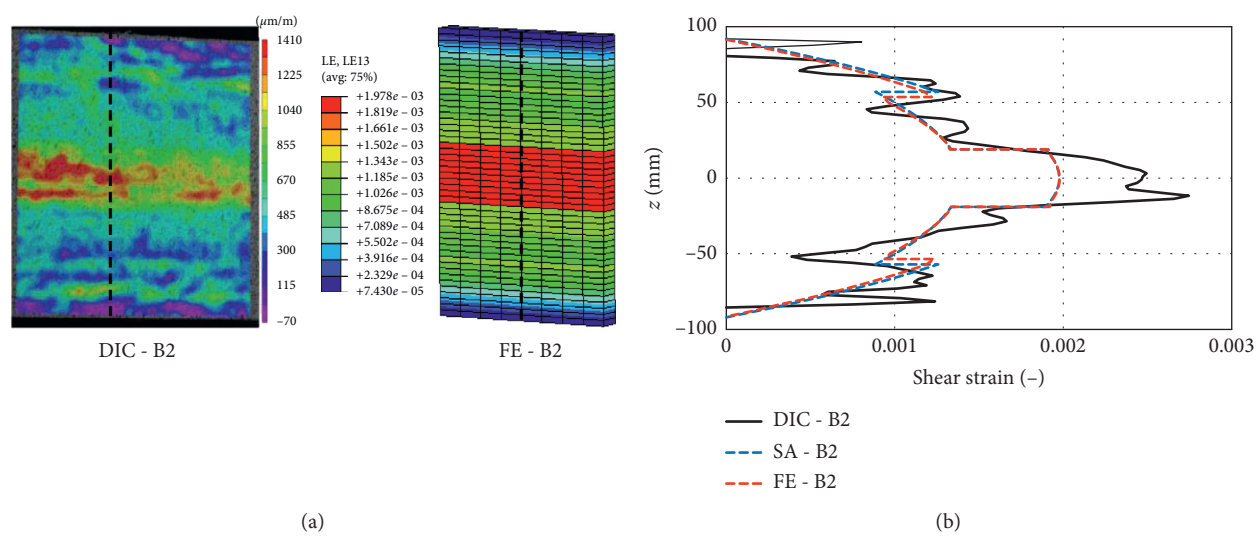

Figure 12: Colour contour plots and shear strain distribution from bending tests for B2.

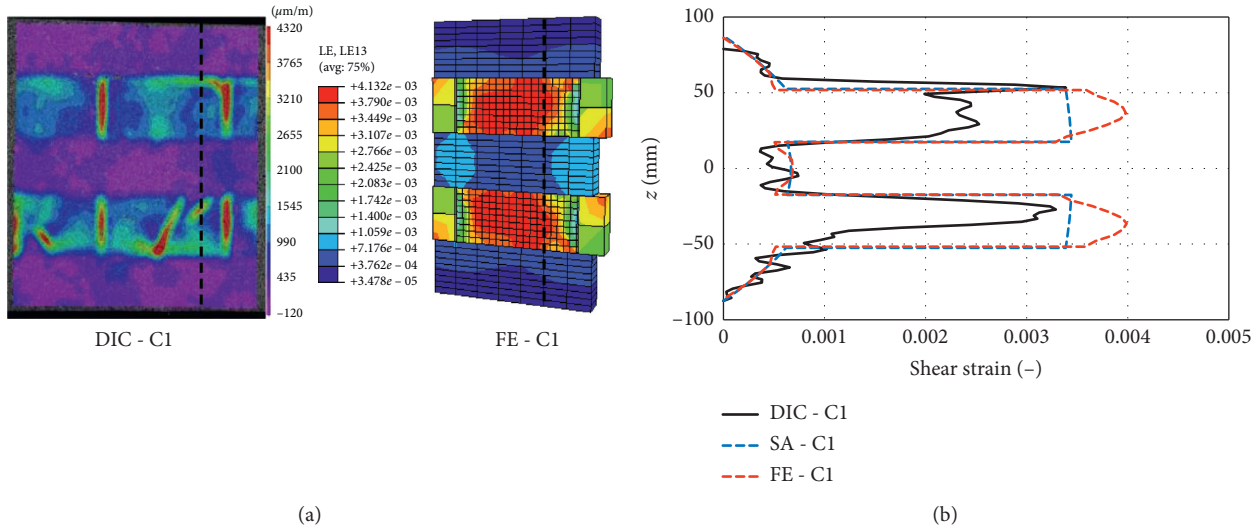

Figure 13: Colour contour plots and shear strain distribution from bending tests for C1.

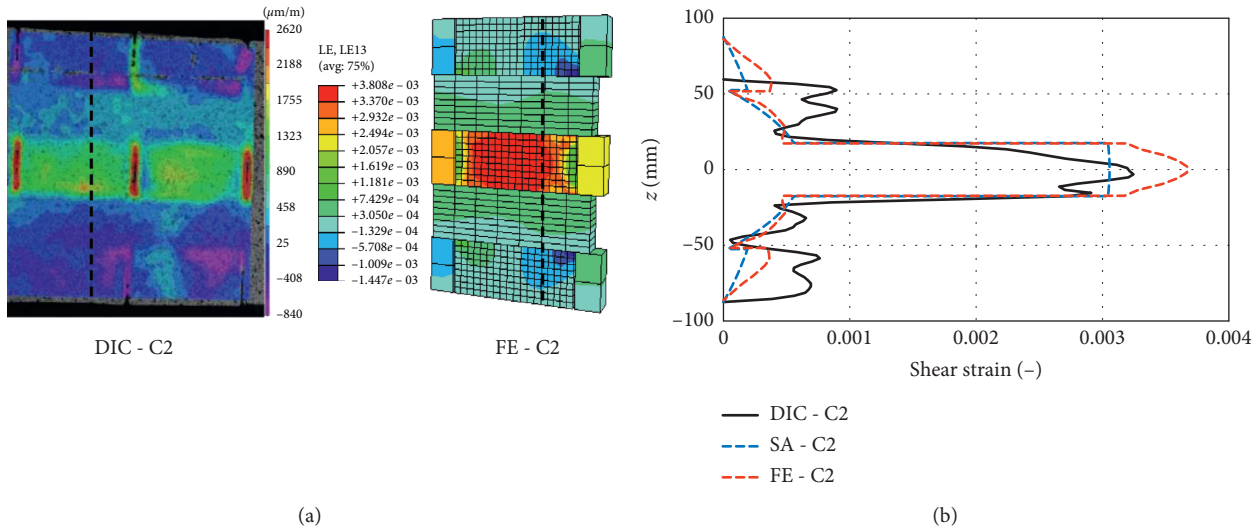

Figure 14: Colour contour plots and shear strain distribution from bending tests for C2.

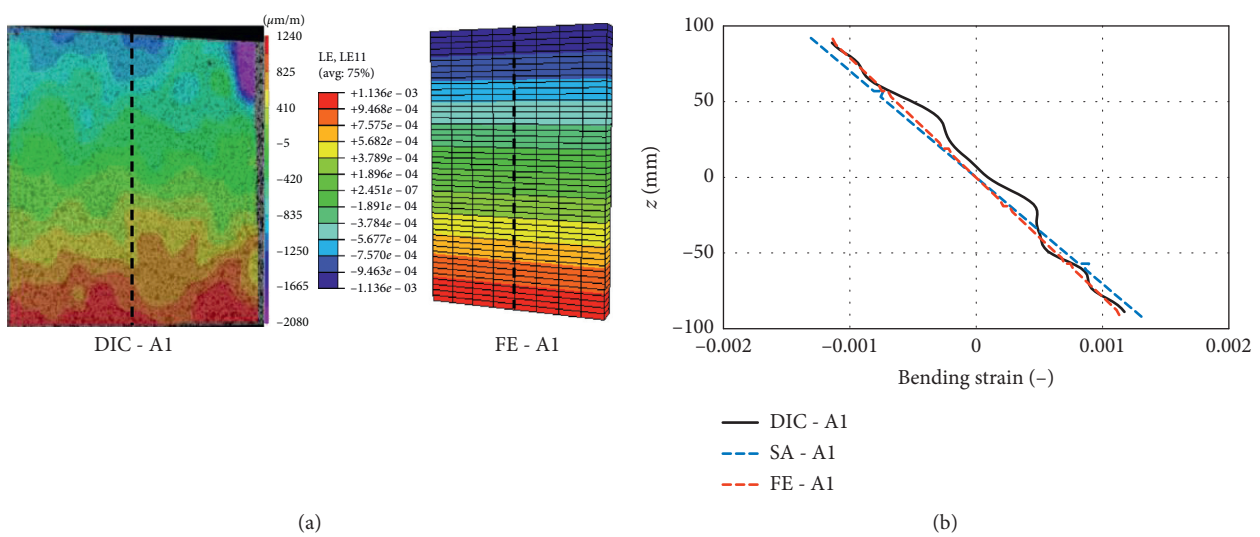

Figure 15: Colour contour plots and normal strain distribution from bending tests for A1.

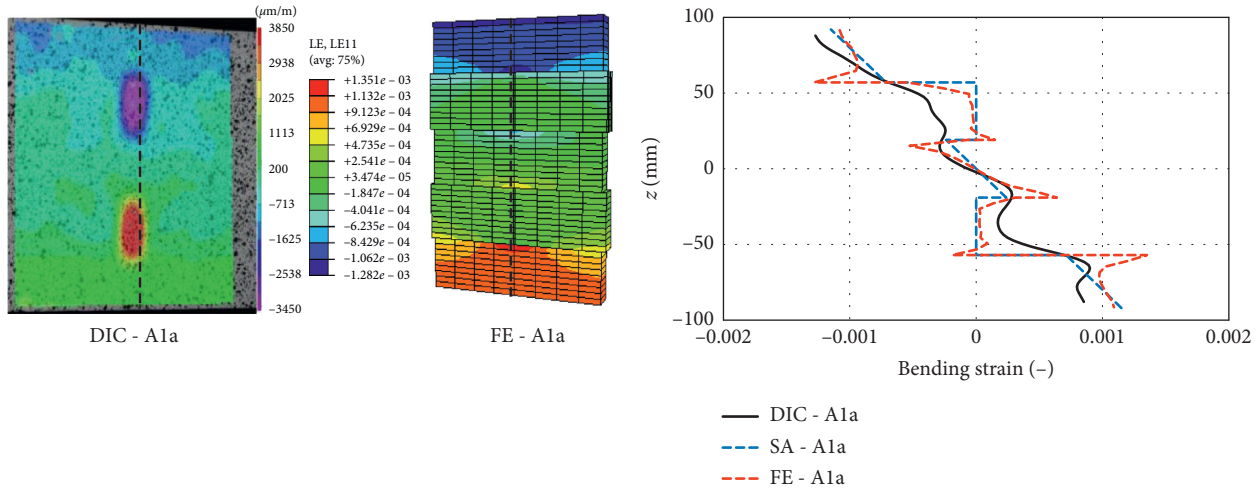

Figure 16: Colour contour plots and normal strain distribution from bending tests for A1a.

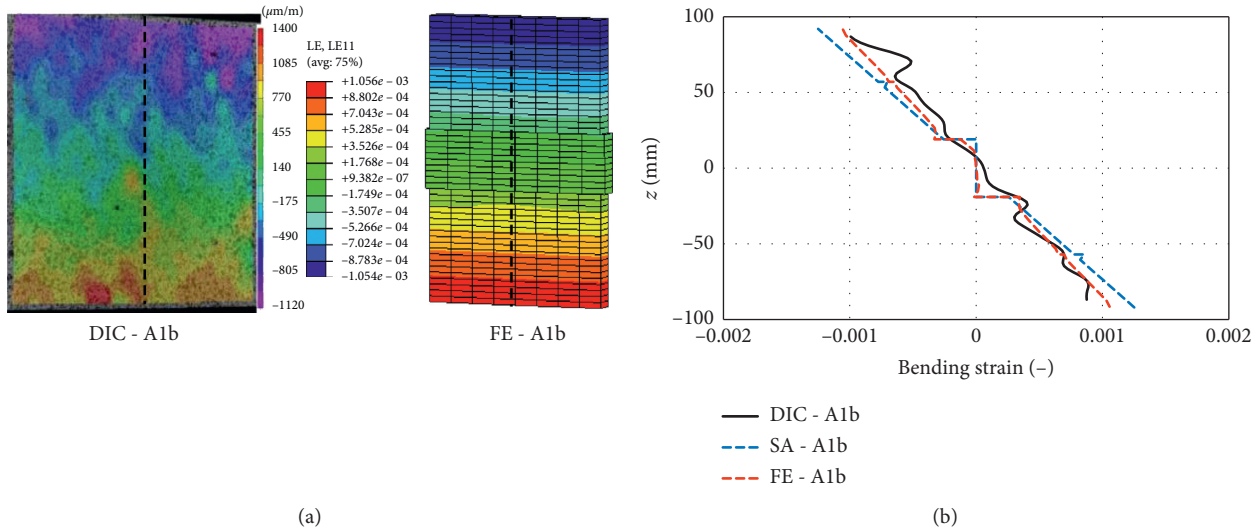

Figure 17: Colour contour plots and normal strain distribution from bending tests for A1b.

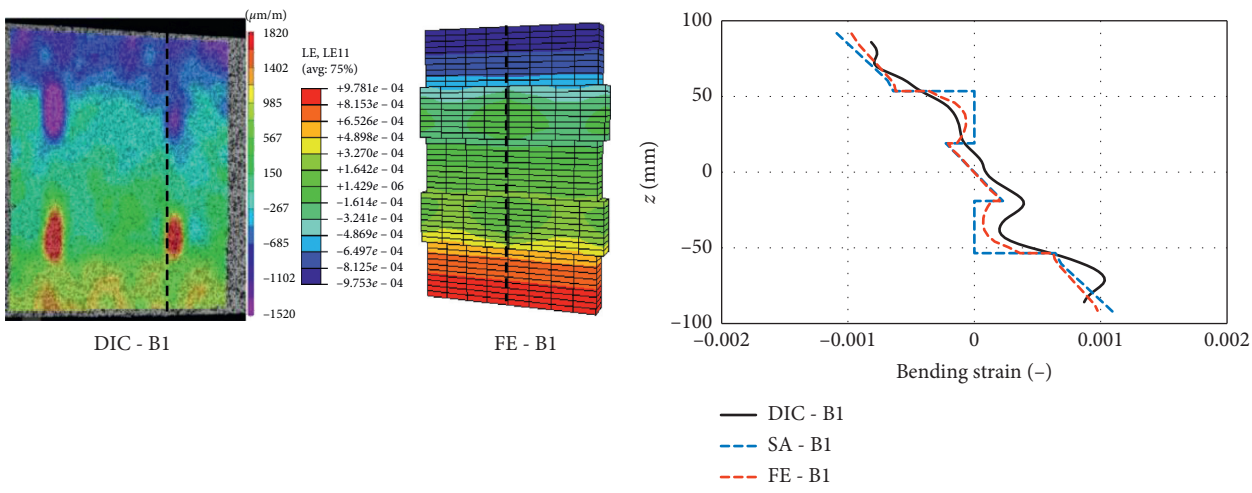

Figure 18: Colour contour plots and normal strain distribution from bending tests for B1.

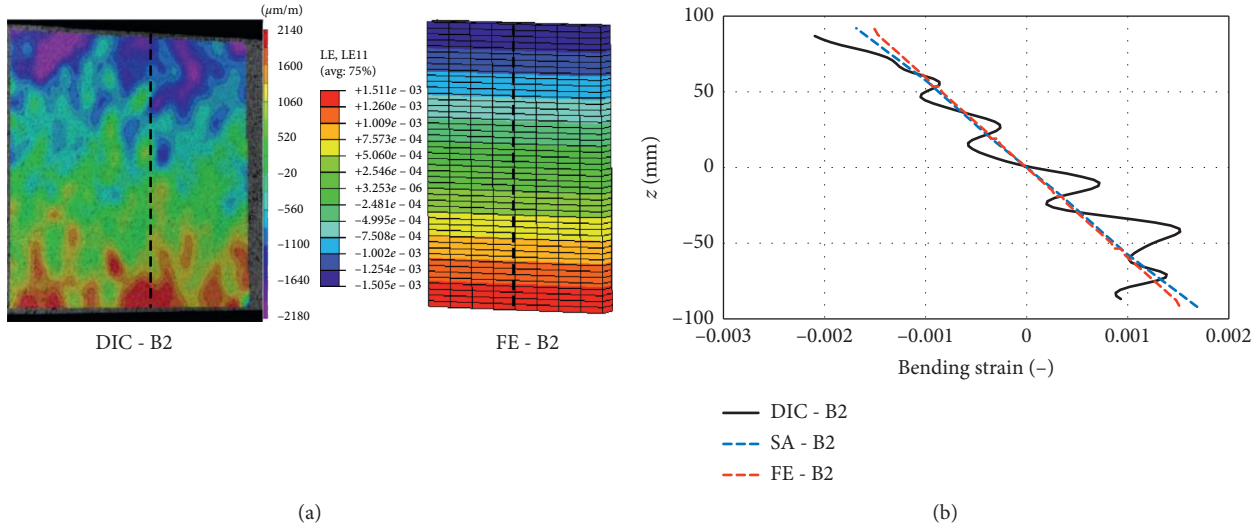

Figure 19: Colour contour plots and normal strain distribution from bending tests for B2.

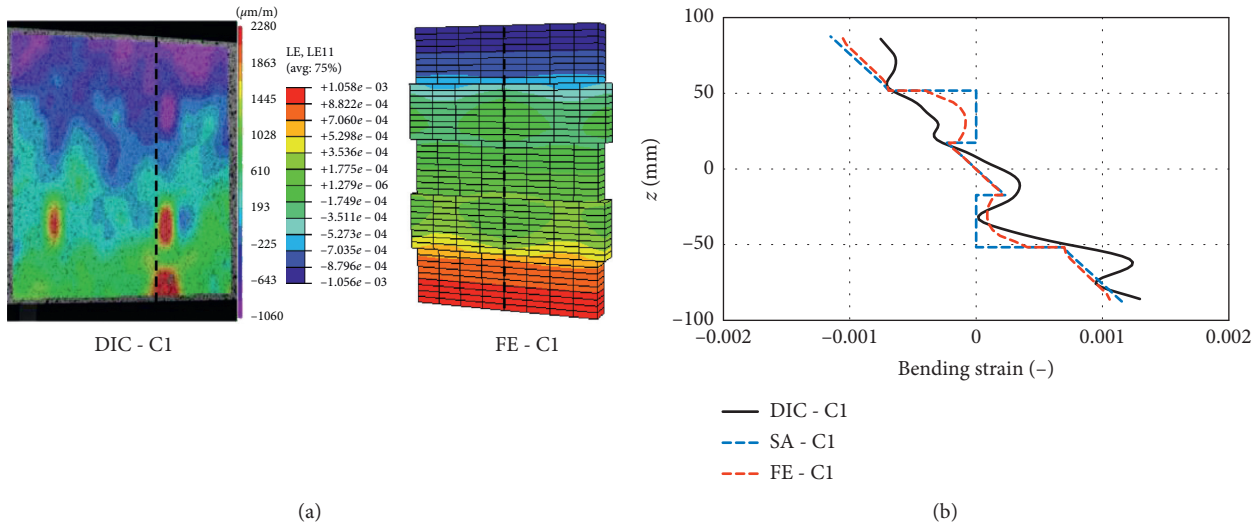

Figure 20: Colour contour plots and normal strain distribution from bending tests for C1.

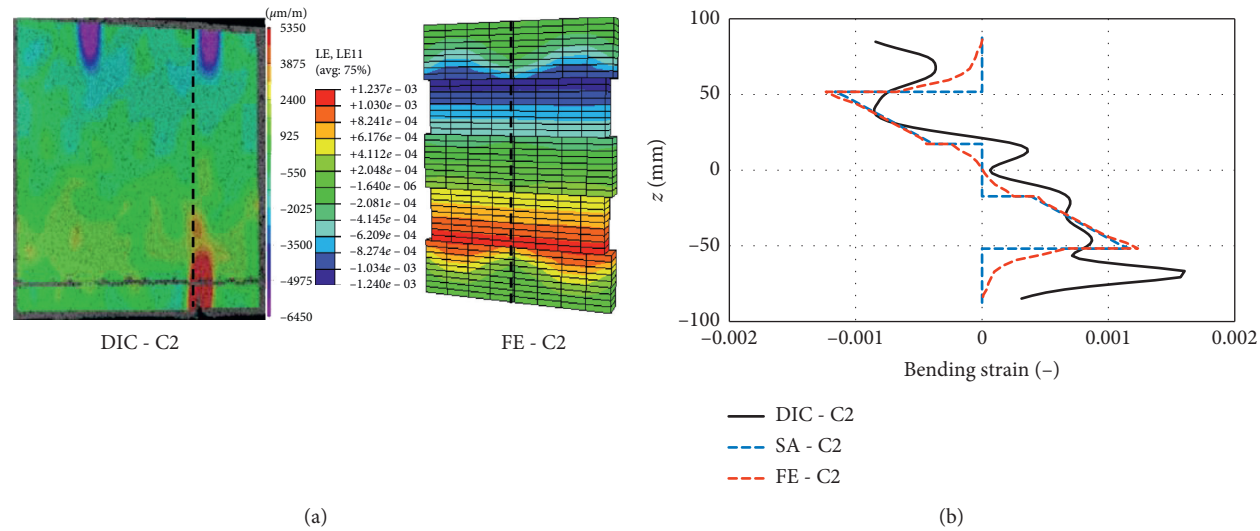

Figure 21: Colour contour plots and normal strain distribution from bending tests for C2.

since all three lay-ups are almost identical, which reflects in the contour plots as well as the diagrams. Figures 11–14 show the information for lay-ups B1, B2, C1, and C2, respectively.

As before, for the shear test related strain evaluations, it can be seen that the colour contour plots of DIC and FE match well. As previously described, the shear strain in the DIC contour plot is presented as Lagrange strain tensors and is therefore about half of the corresponding FE values. Similar to the shear strain DIC contour plots from the shear tests, gaps between laminates (B1, C1, and C2) show high strain areas. As before, this is likely due to the strain evaluation process of the DIC method. Compared to the shear test related shear strain distributions, the shear strain from the bending tests shows a higher level of symmetry with respect to the centre of the cross section ($z = 0$ mm). This has to do with the location of the strain determination. Here, the absence of a nearby induced load or a reaction force leads to a symmetrical strain distribution shape. Besides the missing higher strain towards the bottom lumber-to-LVL glueline, all specimens show the same characteristics that were observed in the shear test related strain distributions.

3.3. Normal Strain in Bending Tests. As shown in Figures 3 and 4, the normal strain measurements from the bending tests were evaluated about halfway between loading points. Figures 15–21 present the data for the lay-ups A1, A1a, A1b, B1, B2, C1, and C2, respectively. It should be noted that all FE results were taken slightly off centre in order to obtain strain values from the edge of the gaps between lamina, while the SA related data was determined within the gaps. This was done since the SA approach only distinguishes between two cases, a solid cross section or a cross section with gaps, but cannot address the strain at the boundaries. This is the case for lay-ups A1a, A1b, B1, C1, and C2.

Similar to the shear strain evaluations, the colour contour plots of DIC and FE show good agreement for the normal strain. Due to the DIC strain evaluation process, gaps between laminates (A1a, A1b, B1, C1, and C2) show as high strain areas. Here, specimens A1, A1a, and A1b are presented separately since the gaps in A1a and A1b are located close to the areas of interest. Based on the distribution of the modulus of elasticity (MOE), specimens A1 and B2 (Figures 15 and 19, respectively) are almost homogeneous. This reflects in the normal strain distributions, where these two specimens show linear behaviour in all three methods. The DIC data of A1, especially, shows good agreement, while the DIC data of B2 shows some deviation from the calculated strain distributions. These variations could have occurred due to the rough surface of the LVL and associated inaccuracies in the DIC measurement. Another reason could be the local variations in MOE. Similar to A1, A1b (Figure 17) shows almost linear behaviour since the installed gap is located close to the neutral axis and therefore the influence of the gap is rather small. For all other specimens with gaps, namely, A1a, B1, C1, and C2 (Figures 16, 18, 20, and 21, respectively), the influence of the gaps is more obvious. It can be seen that both SA and FE show good agreement with the measured DIC data, with the FE distributions generally reflecting the DIC data better in the area of the gaps where the DIC distributions follow a more rounded trend compared to the defined steps of the SA method. It can be seen that the rounded steps of the DIC distributions in the areas of the gaps are larger within the tension zone (bottom half of the cross sections). A reason could be that the gaps in the compression zone (top half of the cross sections) close, thereby transferring forces in contact. Another reason could be different MOE values in compression and tension within the materials [21].

4. Conclusions

Seven (7) different 5-layer composite laminated panels (CLP) and cross-laminated timber (CLT) panels were manufactured and tested as beams in short-span shear tests and third-point bending tests. Shear and normal strain measurements were taken during the tests using the digital imaging correlation (DIC) technique. The strain distributions were compared with distributions calculated based on the shear analogy (SA) method and finite element (FE) analysis.

The results show that the shear analogy method is capable of estimating shear and normal strain distributions in CLP and CLT and therefore the shear and normal stress distributions. In situations where loads are introduced locally or supports induce a rapid change in internal forces due to geometrical constraints, the shear analogy method underestimates local shear strain, which could lead to potential premature failure of the structural element. This is not surprising since the shear analogy method was not developed to determine internal stresses and strains close to local loadings or supports. Here, a determination of the shear strain and stress based on FE analysis might be advisable as the FE results show better agreement with the measured DIC strain in the areas of the supports. In addition, the FE analysis generally shows a closer agreement with the measured strain around gaps within layers as the shear analogy can only distinguish between the gap and no-gap cases, but not the gap boundary case. Furthermore, FE analysis has the potential to include the effects of local reinforcement measures on strain distributions. It should be noted that the accuracy of both shear analogy and FE analysis is highly dependent on the assumed material properties.

Data Availability

The data used to support the findings of this study are available from the corresponding author upon request.

Conflicts of Interest

The authors declare that there are no conflicts of interest regarding the publication of this paper.

Acknowledgments

Funding for the research was provided by the Natural Sciences and Engineering Research Council of Canada (NSERC)

through the Engage Program and Alberta Innovates through its Alberta Bio Future Research and Innovation Program.

References

[1] R. Brandner, G. Flatscher, A. Ringhofer, G. Schickhofer, and A. Thiel, "Cross laminated timber (CLT): overview and development," *European Journal of Wood and Wood Products*, vol. 74, no. 3, pp. 331–351, 2016.

[2] S. Aicher, M. Hirsch, and Z. Christian, "Hybrid cross-laminated timber plates with beech wood cross-layers," *Construction and Building Materials*, vol. 124, pp. 1007–1018, 2016.

[3] W. G. Davids, N. Willey, R. Lopez-Anido et al., "Structural performance of hybrid SPFs-LSL cross-laminated timber panels," *Construction and Building Materials*, vol. 149, pp. 156–163, 2017.

[4] Q. Li, Z. Wang, Z. Liang, L. Li, M. Gong, and J. Zhou, "Shear properties of hybrid CLT fabricated with lumber and OSB," *Construction and Building Materials*, vol. 261, 2020.

[5] N. M. Galih, S. M. Yang, and S. G. Kang, "Study on the mechanical properties of tropical hybrid cross laminated timber using bamboo laminated board as core layer," *Journal of the Korean Wood Science and Technology*, vol. 48, no. 2, pp. 245–252, 2020.

[6] ASTM International, *ASTM D198-15: Standard Test Methods of Static Tests of Lumber in Structural Sizes*, ASTM International, West Conshohocken, PA, USA, 2015.

[7] A. Sandoli and B. Calderoni, "The rolling shear influence on the out-of-plane behavior of CLT panels: a comparative analysis," *Buildings*, vol. 10, no. 3, 2020.

[8] L. Franzoni, A. Lebée, F. Lyon, and G. Forêt, "Elastic behavior of cross laminated timber and timber panels with regular gaps: thick-plate modeling and experimental validation," *Engineering Structures*, vol. 141, pp. 402–416, 2017.

[9] J. Niederwestberg, J. Zhou, and Y. H. Chui, "Mechanical properties of innovative, multi-layer composite laminated panels," *Buildings*, vol. 8, no. 10, 2018.

[10] J. Niederwestberg, J. Zhou, and Y. H. Chui, "Strain distribution of 5-layer composite laminated panels using digital imaging correlation technique," in *Proceedings of the World Conference of Timber Engineering 2018*, Seoul, South Korea, August 2018.

[11] Canadian Standards Association, *CSA O86-19 Engineering Design in Wood*, Canadian Standards Association, Toronto, Canada, 2019.

[12] M. Gong and Y. H. Chui, *Evaluation of Planar Shear Properties of Cross Layer in Massive Timber Panel. Final Report #: WSTC2014-038*, Wood Science and Technology Centre, The University of New Brunswick, Fredericton, Canada, 2015.

[13] Y. H. Chui, M. Gong, and J. Niederwestberg, *"Development of a Lumber-SCL Massive Timber Panel Product, Final Report #: WSTC2014-038*, Wood Science and Technology Centre, The University of New Brunswick, Fredericton, Canada, 2015.

[14] ASTM International, *ASTM D2718-00: Standard Test Methods for Structural Panels in Planar Shear (Rolling Shear)*, ASTM International, West Conshohocken, PA, USA, 2006.

[15] M. A. Sutton, "Digital image correlation for shape and deformation measurements," in *Springer Handbook of Experimental Solid Mechanics*, pp. 565–600, Springer, Berlin, Germany, 2008.

[16] APA-The Engineered Wood Association, *Standard for Performance-Rated Cross-Laminated Timber: ANSI/APA PRG 320*, APA-The Engineered Wood Association, Tacoma, WA, USA, 2017.

[17] Correlated Solutions Incorporated, *Correlated Solutions Homepage*, Correlated Solutions Incorporated, Irmo, SC, USA, 2020, http://www.correlatedsolutions.com.

[18] H. Kreuzinger, "Platten, Scheiben und Schalen–ein Berechnungsmodell für gängige Statikprogramme," *Bauen mit Holz*, vol. 1, pp. 34–39, 1999.

[19] S. Winter, H. Kreuzinger, and P. Mestek, "Flächen aus brettstapeln, brettsperrholz und verbundkonstruktionen," 2008, https://mediatum.ub.tum.de/doc/739585/739585.pdf.

[20] Dassault Systemes, "ABAQUS 6.22 [Computer Software]," 2019.

[21] M. H. Schneider and J. G. Phillips, "Elasticity of wood and wood polymer composites in tension compression and bending," *Wood Science and Technology*, vol. 25, no. 5, pp. 361–364, 1991.